Dyes and Pigments 182 (2020) 108636

Contents lists available at ScienceDirect

Dyes and Pigments

journal homepage: http://www.elsevier.com/locate/dyepig

Boron difluoride functionalized (tetrahydroimidazo[1,5-*a*]pyridin-3-yl) phenols: Highly fluorescent blue emissive materials

Gioele Colombo [a], Antonio Romeo [a], G. Attilio Ardizzoia [a], Julien Furrer [b], Bruno Therrien [c], Stefano Brenna [a,*]

[a] Dipartimento di Scienza e Alta Tecnologia, Università degli Studi dell'Insubria and CIRCC, Via Valleggio, 9, 22100, Como, Italy
[b] Department für Chemie und Biochemie, Universität Bern, Freiestrasse 3, CH-3012, Bern, Switzerland
[c] Institute of Chemistry, Université de Neuchâtel, Avenue de Bellevaux 51, CH-2000, Neuchâtel, Switzerland

ARTICLE INFO

Keywords:
Imidazo[1,5-*a*]pyridines
Fluorescence
Blue emission
Boron

ABSTRACT

Some (tetrahydroimidazo[1,5-*a*]pyridin-3-yl)phenols were reacted with boron trifluoride diethyl etherate and the resulting BF_2-functionalized compounds were fully characterized both in solution using ^{1}H, ^{13}C, ^{11}B, ^{19}F NMR spectroscopy and in the solid state (infrared, fluorescence, X-ray). When excited with UV light these boron difluoride derivatives show in dichloromethane solution an intense fluorescence emission in the UV region, with λ_{max} of emission varying from 357 to 390 nm. Good absolute quantum yields are recorded for most of the compounds. In the solid state, they are characterized by a strong blue emission (388–435 nm), with high absolute quantum yields (up to 0.68) and *x*,*y* color coordinates (CIE 1931) close to those expected for standard blue. Time-Dependent Density Functional Theory (TD-DFT) calculations were used to define the nature of the electronic transitions and excited states involved in the fluorescence process.

1. Introduction

Blue emissive materials represent a key target for many lighting applications, especially for small panel displays. These devices are based on organic light-emitting diodes (OLEDs), which use red, green, and blue emitters, with the latter covering about 50% of the total pixel area of the display. While great success has been achieved in the fabrication of red and green phosphorescent OLEDs (Ph-OLEDs), many efforts are still devoted to obtain a proper blue counterpart. Thus, the search for blue emissive materials suitable for OLEDs application is a constant goal for chemists and material scientists [1–5]. Several approaches have been followed to achieve the required performances. First generation OLEDs use blue emissive fluorescent compounds [1,5], which however limit the internal quantum efficiency (IQE) to 25% due to spin statistics (i.e., 25% singlet *vs*. 75% triplet excitons formed). The incorporation of heavy metals (iridium, platinum) in the emissive layer allows to overcome this problem and leads to more efficient second generation phosphorescent OLEDs [1,4]. However, the use of heavy and costly metals still represents a drawback for these systems. Later, materials characterized by a very low energy gap between singlet (S_1) and triplet (T_1) excited states (ΔE_{ST}) permitted to formally reach a 100% IQE. Indeed, reducing ΔE_{ST} to less than 0.1 eV favors a thermal reverse intersystem crossing (RISC) of triplet excitons to the singlet state, the resulting emission being called thermally activated delayed fluorescence (TADF) [6,7]. Finally, a very recent approach led to a longer operation lifetime for blue OLEDs by means of hybridized local and charge transfer (HLCT) emission [8].

Imidazo[1,5-*a*]pyridines represent interesting heterocyclic compounds widely explored due to their photophysical properties [9]; their most relevant features are large Stokes shift, high quantum yields and a wide range of emission depending on their functionalization [10,11]. Furthermore, there are numerous publications on luminescent transition metal compounds based on imidazo[1,5-*a*]pyridines [12–16]. In the last years, we investigated the photophysical properties of zinc(II) [17–19] and silver(I) [20] complexes with different 3-aryl-substituted imidazo[1,5-*a*]pyridines, whereas more recently we synthesized a series of (tetrahydroimidazo[1,5-*a*]pyridin-3-yl)phenols [21], which showed a bright fluorescence emission characterized by a very high Stokes shift (up to 189 nm, 1.28 eV) and remarkable quantum yields (up to 0.72). The higher performances of these species with respect to the parent non-hydrogenated ones, prompted us to further investigate their emissive properties by introducing a BF_2 fragment within their skeleton. Indeed, boron containing compounds proved to be a highly promising

* Corresponding author.
E-mail address: stefano.brenna@uninsubria.it (S. Brenna).

https://doi.org/10.1016/j.dyepig.2020.108636
Received 21 February 2020; Received in revised form 2 June 2020; Accepted 3 June 2020
Available online 27 June 2020

class of building blocks for optoelectronic materials [22–24]; specifically, boron dipyrromethene (BODIPY) derivatives [25] showed relevant fluorescence properties and have found applications in several fields [26], including optoelectronic materials like OLEDs [27] and organic photovoltaic (OPV) devices [28]. The introduction of a BF_2 fragment in compounds with *N,O*- chelation [29,30] increased the photoluminescence performances as well; however, only a couple of reports on boron difluoride complexes of imidazo[1,2-*a*]pyridines [31] and imidazo[1,5-*a*]pyridines [32] have been published so far, which encouraged us to further develop the chemistry of (tetrahydroimidazo [1,5-*a*]pyridin-3-yl)phenols with boron trifluoride. The resulting boron-containing derivatives have been fully characterized (including ^{19}F and ^{11}B NMR and X-ray). They all showed intense UV-to-blue fluorescence emission, with a general enhanced efficiency with respect to the free counterparts. Measured lifetimes were in the range 1.1–1.4 ns in solution and slightly longer in the solid state (about 6 ns). The photophysical behavior of thin layer of these compounds dispersed in a host polymeric matrix is also discussed.

2. Materials and methods

2.1. General remarks

Infrared spectra were acquired on a Shimadzu Prestige-21 spectrophotometer with a 1 cm^{-1} resolution. Elemental analyses were obtained with a PerkinElmer CHN Analyzer 2400 Series II. NMR spectra were recorded with an AVANCE III HD Bruker spectrometer operating at 400 MHz for ^1H NMR, 100 MHz for $^{13}C\{^1H\}$ NMR, 376 MHz for ^{19}F NMR and 128 MHz for ^{11}B NMR. Chemical shifts are given as δ values in ppm relative to residual solvent peaks as the internal reference. *J* values are given in Hz. High-pressure experiments were conducted using a 100 ml PARR stainless steel autoclave reactor equipped with an Ashcroft Duralife (3000 psi) pressure gauge and a PARR 4842 temperature controller. The UV–vis, excitation and emission spectra were measured using a fluorescence spectrometer (Edinburgh Instruments FS5) equipped with a 150 W continuous Xenon lamp as a light source and were corrected for the wavelength response of the instrument; lifetime measurements were performed on the same FS5 Edinburgh Instruments equipped with a EPLED-320 (Edinburgh Instruments) as the pulsed source. Absolute fluorescence quantum yields in solution were determined using a PhotoMed GmbH K-Sphere Integrating Sphere (3.2 inch. diameter). Analysis of the lifetime decay curve and determination of absolute quantum yields were done using Fluoracle® Software package (Ver. 1.9.1), which runs the FS5 instrument. Absolute fluorescence quantum yields in solid state were measured on a Photon Technology International (PTI) QuantaMaster QM-40 spectrometer (equipped with a Xe arc lamp, 70 W), using the abovementioned PhotoMed GmbH K-Sphere Integrating Sphere (3.2 inch. diameter). The integrated luminescence areas were obtained by the Felix32™ analysis software and used to determine the absolute PLQYs (Φ_{PL}, uncertainties of ±5%) according to the literature [33]. (Tetrahydroimidazo[1,5-*a*]pyridin-3-yl) phenols (**^{R}TIPP**; R = H, Me, OMe, F) were prepared as previously reported [21]; all chemicals were of reagent grade quality, were purchased commercially (Acros, TCI Chemicals, Fluorochem), and used as received.

2.2. Synthesis of ^{OH}TIPP

The hydroxy substituted (tetrahydroimidazo[1,5-*a*]pyridin-3-yl) phenol **^{OH}TIPP** was prepared in two steps following a published procedure [21]. *Step A*: 2-acetylpyridine (2 mL, 1.85 g, 1 eq), ammonium acetate (6.88 g, 5 eq) and 2,5-dihydroxybenzaldehyde (4.89 g, 2 eq) were dissolved in 40 mL of deoxygenated glacial acetic acid. The resulting yellow-orange suspension was left stirring under inert atmosphere for 1 week. During this time, precipitation of a solid occurred, and the suspension turned to deep red. The solid was filtered, washed with acetic acid and discarded. The organic phase was extracted with dichloromethane (4 x 100 mL), washed with an aqueous saturated solution of sodium hydrogen carbonate and dried over sodium sulfate. The solvent was removed under reduced pressure to afford a yellow-orange oil that was triturated wit hexane. The solid obtained was filtered, washed with water and dried under vacuum. *Step B*: In a Parr steel autoclave previously purged with argon, 30 mL of CH_3OH were thoroughly deoxygenated with argon, then the yellow solid obtained in step A (1 g) and 10% Pd/C (0.1 g) were added and the suspension further deoxygenated with argon for 30 min. Then the autoclave was carefully charged with 10 atm of hydrogen and the system was maintained under stirring at room temperature for 72 h. The suspension was filtered over a pad of Celite to remove the catalyst and the organic phase was concentrated to dryness until an oil was obtained. Addition of diethylether afforded a light brown solid, which was filtered and dried under vacuum. See Supporting for complete experimental data.

2.3. General procedure for the synthesis of boron difluoride compounds ^{R}TIPP_BF$_2$

(Tetrahydroimidazo[1,5-*a*]pyridin-3-yl)phenols **^{R}TIPPs** (1 g, 1 eq) were dissolved in 8 mL of deoxygenated dichloromethane, then $BF_3{\cdot}Et_2O$ (1.35 mL, 2.5 eq) was added dropwise. Addition of Et_3N (730 μL, 1.2 eq) led to the formation of a pale orange solution, which was stirred at room temperature for 12 h. During this time, precipitation of a solid occurred. Then the solvent was reduced to half the volume, and the solid was filtered off. This crude product was dissolved in a minimum amount of CH_2Cl_2 (5 mL) and the solution was passed over a pad of SiO_2 to remove the last traces of Et_3NHF. The filtrate was concentrated to dryness, giving the desired products as white solids.

2.3.1. ^{H}TIPP_BF$_2$

Yield: 0.91 g (75.0%). Anal. Calcd for $C_{14}H_{15}BF_2N_2O$ (%): C, 60.90; H, 5.48; N, 10.14. Found (%): C, 60.87; H, 5.52; N, 10.30. ^1H NMR (400 MHz, CD_2Cl_2, 25 °C): δ = 7.76 (dd, *J* = 8.1, 1.6 Hz, 1H), 7.45–7.40 (m, 1H), 7.16 (dd, *J* = 8.3, 1.2 Hz, 1H), 7.04–6.99 (m, 1H), 4.38 (t, *J* = 6.2 Hz, 2H), 2.87–2.78 (m, 2H), 2.34 (s, *J* = 1.1 Hz, 3H), 2.17–2.06 (m, 2H), 2.00–1.89 (m, 2H). ^{13}C NMR (100 MHz, CD_2Cl_2, 25 °C): δ = 131.85, 123.76, 119.82, 119.12, 46.70, 22.97, 20.51, 18.69, 8.90. ^{19}F NMR (376 MHz, CD_2Cl_2, 25 °C): δ = −139.09 (q, *J* = 14.9 Hz). ^{11}B NMR (128 MHz, CD_2Cl_2, 25 °C): δ = 0.78 (t, *J* = 15.4 Hz). IR (nujol mull) $\tilde{\nu}$ = 1032–1162 cm^{-1} (BF_2).

2.3.2. ^{Me}TIPP_BF$_2$

Yield: 0.95 g (78.5%). Anal. Calcd for $C_{15}H_{17}BF_2N_2O$ (%): C, 62.10; H, 5.91; N, 9.66. Found (%): C, 62.11; H, 6.03; N, 9.72. ^1H NMR (400 MHz, CD_2Cl_2) δ 7.54 (d, *J* = 2.1 Hz, 1H), 7.25 (dd, *J* = 8.3, 2.1 Hz, 1H), 7.05 (d, *J* = 8.4 Hz, 1H), 4.39 (t, *J* = 6.2 Hz, 2H), 2.83 (m, 2H), 2.33 (s, 1H), 2.17–2.06 (m, 2H), 2.00–1.89 (m, 2H). ^{13}C NMR (100 MHz CD_2Cl_2) δ 153.62, 132.76, 128.43, 126.03, 125.15, 123.71, 119.50, 110.25, 46.74, 22.98, 20.57, 18.73, 8.91. ^{19}F NMR (376.5 MHz, CD_2Cl_2) δ −139.36 (q, *J* = 15.1 Hz). ^{11}B NMR (128 MHz, CD_2Cl_2) δ 0.81 (t, *J* = 15.4 Hz). IR (nujol mull) $\tilde{\nu}$ = 1034–1168 cm^{-1} (BF_2).

2.3.3. ^{OMe}TIPP_BF$_2$

Yield: 0.89 g (74.4%). Anal. Calcd for $C_{15}H_{17}BF_2N_2O_2$ (%): C, 58.85; H, 5.60; N, 9.15. Found (%): C, 58.23; H, 5.63; N, 9.05. ^1H NMR (400 MHz, CD_2Cl_2, 25 °C): δ = 7.23 (d, *J* = 2.8 Hz, 1H), 7.06 (d, *J* = 9.0 Hz, 1H), 7.00 (dd, *J* = 9.0, 2.9 Hz, 1H), 4.35 (t, *J* = 6.2 Hz, 2H), 3.80 (s, 3H), 2.79 (t, *J* = 6.3 Hz, 2H), 2.29 (s, 3H), 2.16–1.96 (m, 2H), 1.96–1.82 (m, 2H). ^{13}C NMR (100 MHz, CD_2Cl_2, 25 °C): δ = 152.24, 120.26, 117.68, 114.99, 109.11, 55.97, 46.57, 22.94, 20.52, 18.70, 8.92. ^{19}F NMR (376 MHz, CD_2Cl_2, 25 °C): δ = −139.63 (q, *J* = 14.9 Hz). ^{11}B NMR (128 MHz, CD_2Cl_2, 25 °C): δ = 0.84 (t, *J* = 15.9 Hz). IR (nujol mull) $\tilde{\nu}$ = 1038 - 1103 cm^{-1} (BF_2).

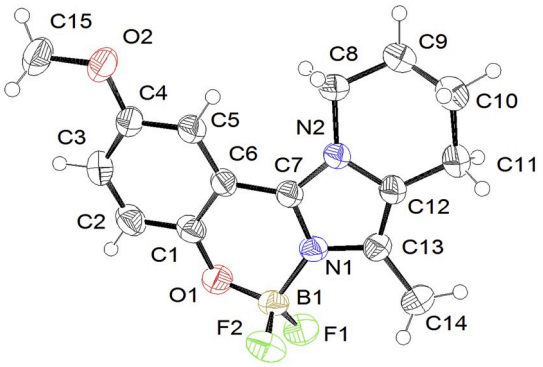

Fig. 1. ORTEP representation of ^{OMe}**TIPP_BF$_2$** at 50% probability level ellipsoids, with atom labeling scheme. Selected bond lengths (Å) and angles (°): B(1)–N(1) 1.561(5), B(1)–O(1) 1.429(5); B(1)–F(1) 1.383(4), B(1)–F(2) 1.391(5); O(1)-B(1)-N(1) 108.9(3), O(1)-B(1)-F(1) 108.8(3), O(1)-B(1)-F(2) 111.8(3), N(1)-B(1)-F(1) 110.3(3), N(1)-B(1)-F(2) 107.8(3), F(1)-B(1)-F(2) 109.2(3).

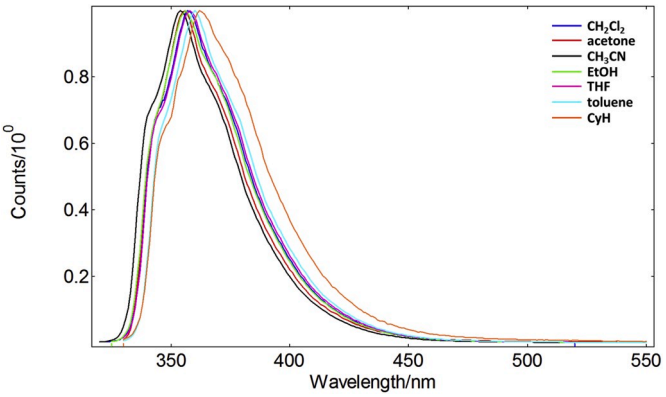

Fig. 2. Normalized emission spectra of compound ^{H}**TIPP_BF$_2$** recorded in solution ($5{\cdot}10^{-5}$ M) in different solvents.

Table 1
Photophysical data for compound ^{H}**TIPP_BF$_2$** recorded in solution ($5{\cdot}10^{-5}$ M) in different solvents.

R = H	λ_{abs} (nm)	λ_{exc} (nm)	λ_{em} (nm)	Stokes shift (eV)	Φ_{PL}	τ (ns)
CH_2Cl_2	319	319	357	0.41	0.54	1.3
acetone	331	333	356	0.24	0.27	1.3
CH_3CN	316	316	354	0.42	0.41	1.5
EtOH	317	318	356	0.42	0.34	1.4
THF	320	320	358	0.41	0.31	1.4
toluene	322	323	360	0.39	0.46	1.3
cyclohexane	261, 323	324	362	0.40	0.17	1.2

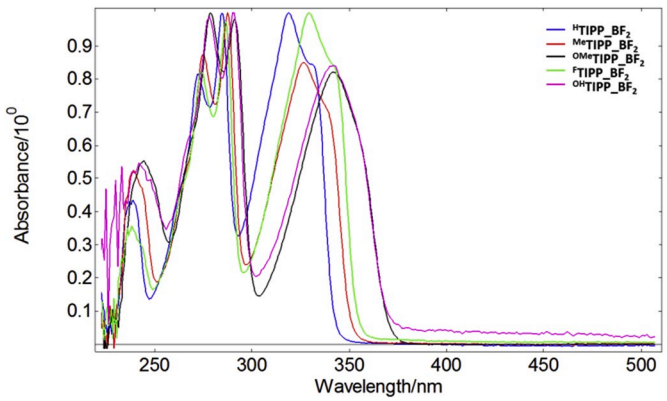

Fig. 3. Normalized UV–vis spectra of ^{R}**TIPP_BF$_2$** compounds (CH_2Cl_2, $5{\cdot}10^{-5}$ M).

2.3.4. ^{F}*TIPP_BF$_2$*

Yield: 0.78 g (65.1%). Anal. Calcd for $C_{14}H_{14}BF_3N_2O$ (%): C, 57.18; H, 4.80; N, 9.53. Found (%): C, 57.17; H, 4.94; N, 9.27. ^{1}H NMR (400 MHz, CD_2Cl_2, 25 °C): δ = 7.42 (dd, J = 9.6, 2.7 Hz, 1H), 7.20–6.99 (m, 2H), 4.32 (t, J = 6.2 Hz, 2H), 2.79 (t, J = 6.5, 2H), 2.30 (s, 3H), 2.17–2.02 (m, 2H), 2.03–1.76 (m, 2H). ^{13}C NMR (100 MHz, CD_2Cl_2, 25 °C): δ = 156.60, 154.25, 151.95, 126.75, 125.67, 120.93, 118.81, 109.55, 46.51, 22.83, 20.51, 18.60, 8.90. ^{19}F NMR (376 MHz, CD_2Cl_2, 25 °C): δ = −124.51 (q, J = 8.4 Hz), −139.14 (q, J = 14.5 Hz). ^{11}B NMR (128 MHz, CD_2Cl_2, 25 °C): δ = 0.79 (t, J = 15.3 Hz). IR (nujol mull) $\tilde{\nu}$ = 1037 - 1168 cm^{-1} (BF_2).

2.3.5. ^{OH}*TIPP_BF$_2$*

Yield: 1.04 g (87%). Anal. Calcd for $C_{14}H_{15}BF_2N_2O_2$ (%): C, 57.57; H, 5.18; N, 9.59. Found (%): C, 60.65; H, 5.21; N, 9.62. ^{1}H NMR (400 MHz, Acetone-d_6) δ 8.03 (s), 7.35 (d, J = 2.7 Hz, 1H), 7.10–6.69 (m, 2H), 4.48 (t, J = 6.2 Hz, 2H), 2.84 (t, J = 6.6 Hz, 2H), 2.79 (s, 1H), 2.26 (t, J = 1.1 Hz, 3H), 2.21–2.11 (m, 2H), 2.00–1.87 (m, 2H). ^{13}C NMR (100 MHz, Acetone-d_6) δ 149.37, 126.51, 124.48, 119.85, 119.24, 109.79, 46.43, 22.68, 20.21, 18.42, 8.32. ^{19}F NMR (376.5 MHz, Acetone-d_6) δ −138.94 (q, J = 14.2 Hz). ^{11}B NMR (128 MHz, Acetone-d_6) δ 0.88 (t, J = 15.1 Hz). IR (nujol mull) $\tilde{\nu}$ = 1032 - 1173 cm^{-1} (BF_2), 3482 cm^{-1} (OH).

2.4. *Single-crystal X-ray structure analysis*

A crystal of ^{OMe}**TIPP_BF$_2$** was mounted on a Stoe Image Plate Diffraction system equipped with a φ circle goniometer, using Mo-Kα graphite monochromated radiation (λ = 0.71073 Å) with φ range 0–200°. The structure was solved by direct methods using the program SHELXS [34], while refinement and all further calculations were carried out using SHELXL [35]. The H-atoms were included in calculated positions and treated as riding atoms using the SHELXL default parameters. The non-H atoms were refined anisotropically, using weighted

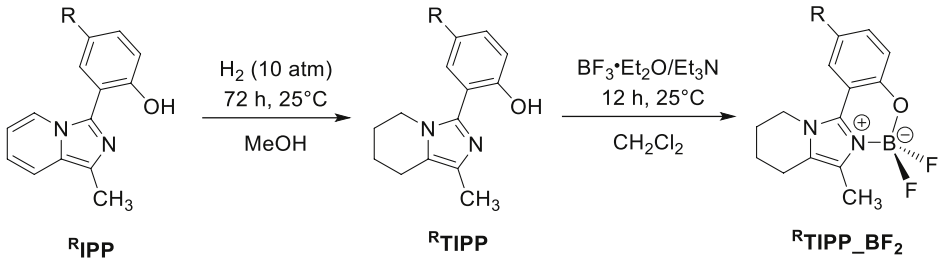

Scheme 1. Catalytic hydrogenation of (imidazo[1,5-*a*]pyridine-3-yl)phenols ^{R}**IPPs** leading to the corresponding (tetrahydroimidazo[1,5-*a*]pyridin-3-yl)phenols ^{R}**TIPPs** and subsequent introduction of the BF_2 fragment.

Table 2
Photophysical data for boron difluoride complexes ^{R}**TIPP_BF$_2$** in dichloromethane solution ($5{\cdot}10^{-5}$ M).

R	λ_{abs} (nm)	ε (M^{-1} cm^{-1})	λ_{exc} (nm)	λ_{em} (nm)	Stokes shift (eV)	Φ_{PL}	τ (ns)	k_r ($\cdot10^8$ s^{-1})	k_{nr} ($\cdot10^8$ s^{-1})
H	319	142380	319	357	0.41	0.54	1.3	4.29	3.65
Me	326	101320	326	367	0.42	0.47	1.3	3.76	4.24
OMe	342	111540	342	390	0.45	0.49	1.4	3.43	3.57
F	329	89320	329	369	0.41	0.30	1.1	2.80	6.54
OH	342	18070	341	388	0.44	0.31	1.4	2.21	4.93

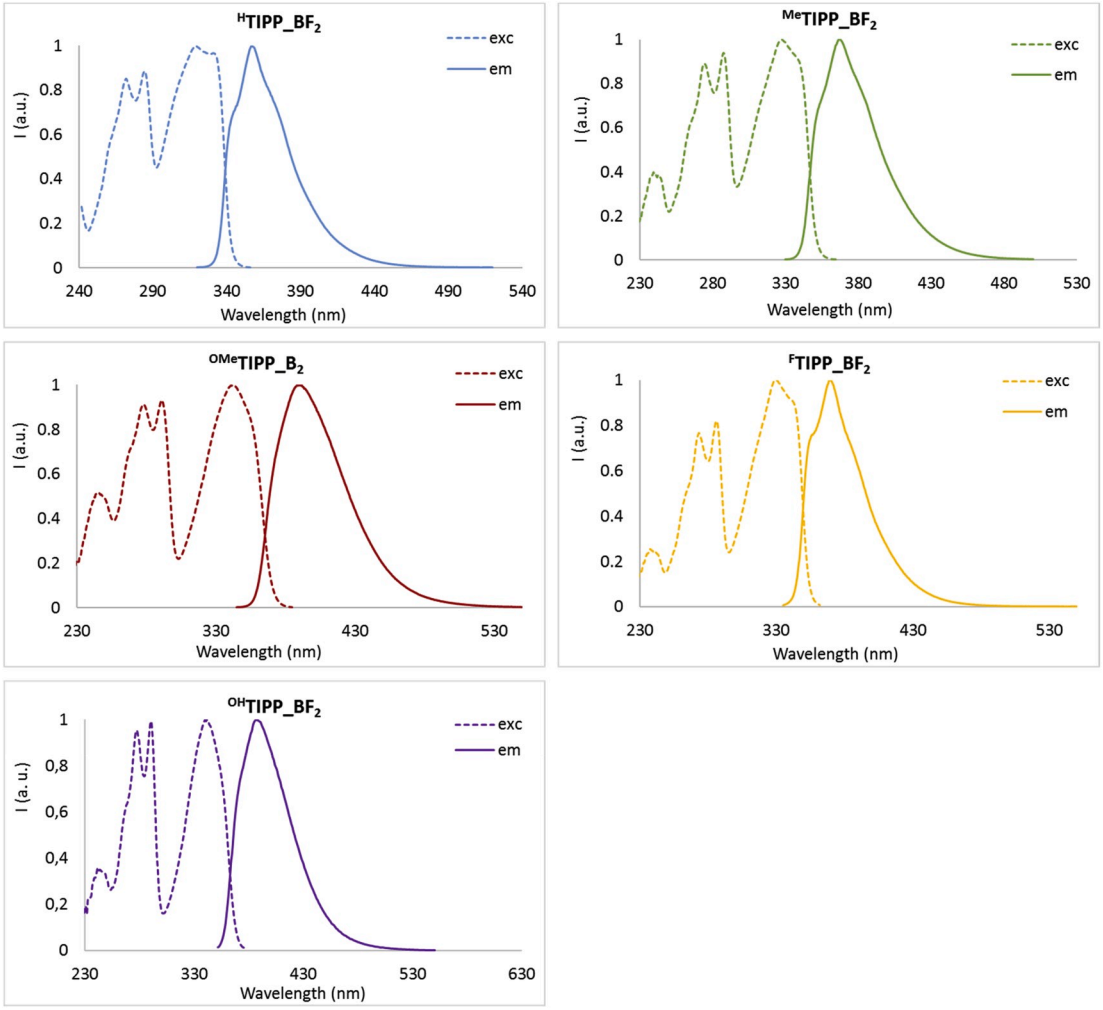

Fig. 4. Normalized excitation (dashed) and emission (solid) spectra of ^{R}**TIPP_BF$_2$** compounds recorded in solution (CH_2Cl_2, $5{\cdot}10^{-5}$ M).

full-matrix least-square on F^2. Crystallographic details are summarized in Table S1. Fig. 1 was drawn with ORTEP–32 [36].

CCDC-1984499 contains the supplementary crystallographic data for this paper. These data can be obtained free of charge via www.ccdc.cam.ac.uk/data_request/cif, by e-mailing data_request@ccdc.cam.ac.uk, or by contacting The Cambridge Crystallographic Data Centre, 12, Union Road, Cambridge CB2 1EZ, UK; fax: +44 1223 336033.

2.5. Computational details

All calculations were carried out at the density functional (DFT) level of theory with the ADF2018.105 program package [37]. The PBE functional plus a D3 dispersion correction energy term (PBE-D3) [38] was employed for all calculations. Frequency analyses were performed for all optimized structures to establish the nature of the stationary points. TD-DFT implemented in the ADF package was used to determine the excitation energies: the 40 lowest singlet-singlet excitations were calculated by using the optimized geometries. For geometry optimizations B, C, H, N, O and F atoms were described through TZ2P basis sets [triple-ξ Slater-type orbitals (STOs) plus two polarization functions]. The corresponding augmented basis set was employed in TD-DFT calculations [39]. Restricted formalism, no-frozen-core approximation (all-electron) and no-symmetry constrains were used in all calculations. Solvent effects (CH_2Cl_2) were simulated employing the conductor-like continuum solvent model (COSMO) [40] as implemented in the ADF suite.

3. Results and discussion

3.1. Synthesis and characterization

The starting (tetrahydroimidazo[1,5-*a*]pyridin-3-yl)phenols ^{R}**TIPP** [21] were prepared by catalytic hydrogenation (Pd/C 10%, 10 atm H_2) of the corresponding (imidazo[1,5-*a*]pyridin3-yl)phenols ^{R}**IPP** [41]

Table 3
Photophysical data for boron difluoride complexes ^{R}**TIPP_BF$_2$** in the solid state and when dispersed in a host polymeric matrix (poly(methyl methacrylate), PMMA).

R	solid state				thin layer (PMMA)			
	λ_{exc} (nm)	λ_{em} (nm)	Φ_{PL}	τ (ns) (% rel)	λ_{exc} (nm)	λ_{em} (nm)	Φ_{PL}	τ (ns) (% rel)
H	343	430	0.68	6.1	318	358	0.25	1.2 (85%) 4.4 (15%)
Me	353	435	0.63	6.9	325	369	0.16	1.0 (77%) 2.8 (23%)
OMe	368	411	0.35	1.7 (43%) 5.4 (57%)	340	391	0.16	1.3 (64%) 2.9 (36%)
F	354	406	0.47	5.6	328	371	0.19	1.3 (83%) 4.6 (17%)
OH	364	388	0.15	0.5 (44%) 2.4 (25%) 7.5 (31%)	343	394	0.13	1.2 (54%) 2.5 (46%)

(Scheme 1). The boron difluoride derivatives were easily obtained by reaction of ^{R}**TIPP** with boron trifluoride diethyl etherate, in the presence of triethylamine, in dichloromethane at room temperature (Scheme 1).

The purity of the products was assessed via elemental analysis and solution NMR: in the ^{1}H NMR spectra of ^{R}**TIPP_BF$_2$** (CD_2Cl_2, 25 °C) the multiplets relative to methylene groups were detected respectively at about 4.35, 2.80, 2.15 and 1.90 ppm. The corresponding resonances in the ^{13}C NMR appear at about 46.6, 22.9, 20.5 and 18.7 ppm (see Figs. S1–S24 in Supporting Information for full spectra). The ^{19}F NMR (CD_2Cl_2, 25 °C) shows a typical splitting consisting of four equidistant lines close to −140 ppm, with a $J_{F\text{-}B} \approx 15$ Hz due to the coupling with the ^{11}B nucleus (Figs. S3–S20). The small unresolved resonance appearing upfiled at the bottom of the main ^{19}F resonance is attributed to the resonance of ^{19}F bound to ^{10}B. The ^{11}B NMR (CD_2Cl_2, 25 °C) shows a triplet centered around 0.5–1.0 ppm, with again a $J_{F\text{-}B} \approx 15$ Hz (Figs. S4–S20). The shape of this signal is indicative of the presence of two equivalent fluorine atoms, as expected for a tetrahedral geometry around the boron atom. This feature was later confirmed by single-crystal X-ray structure analysis (*vide infra*). The infrared spectra (nujol) are characterized by intense stretching vibrations between 1000 and 1200 cm^{-1} associated to the BF_2 system (Figs. S25–S29).

3.2. Single-crystal X-ray structure analysis

The methoxy substituted boron difluoride compound ^{OMe}**TIPP_BF$_2$** was characterized via single-crystal X-ray structure analysis (Fig. 1). As expected, the (tetrahydroimidazo[1,5-*a*]pyridin-3-yl)phenol is *N*,*O*-chelated to boron, which then shows a tetrahedral geometry with a NOF_2 environment. Distances and angles are in accordance with those reported in the literature for comparable *N*,*O*–BF_2 systems [31,32]. As already observed for similar compounds [32], the structure shows a nearly planar arrangement between the imidazolyl ring and the phenolic residue, with the planes identified by these two rings being tilted by 9.11° (Fig. S31). The piperidinic part of the molecule displays a half-chair conformation, with C9 clearly out of the N2–C8–C10–C11–C12 plane (Fig. S32). Despite this half-chair conformation and the tetrahedral geometry of the boron atom, the ^{OMe}**TIPP_BF$_2$** molecules are forming along the *a* axis, π-π head-to-tail stacks of molecules, with centroid-centroid distances between the phenyl and imidazolyl rings being 3.88 Å (Fig. S33).

3.3. Optical properties

First, in order to evaluate any possible solvent effect on the photophysical properties of our compounds, we recorded the UV–vis, excitation and emission spectra of a 0.05 mM solution of compound ^{H}**TIPP_BF$_2$** (taken as a reference of the series) in solvents of different polarity (dichloromethane, acetone, acetonitrile, ethanol, tetrahydrofuran, toluene, cyclohexane). The UV–vis spectra are quite similar (Fig. S34) with two main absorptions at about 270–280 nm and around 320 nm. Only those recorded in acetone and cyclohexane are different: in acetone, the spectrum is influenced by the strong solvent absorption at about 270 nm and shows only one main band at 330 nm. In cyclohexane, where compound ^{H}**TIPP_BF$_2$** resulted very faintly soluble, the main absorption is centered at 260 nm, with the transition at 330 nm appearing only as a broad, low-intensity band. The excitation spectra largely reproduce the UV–vis traces, thus being almost comparable to each other as well (Fig. S35). Again, the only exception is represented by the sample measured as acetone solution, characterized by the expected strong transition at 333 nm. Regarding the emission spectra, their shapes are nearly identical (Fig. 2), whereas a slight bathochromic shift of emission λ_{max} with decreasing solvent polarity is observed. Nevertheless, as demonstrated by the photophysical data reported in Table 1, compound ^{H}**TIPP_BF$_2$** constantly shows an intense blue fluorescence emission centered at about 355 nm in the different solvents, without experiencing any quenching or dramatic shift of emission λ_{max} or its intensity. In all cases, mono-exponential lifetime decays characterized by τ values ranging from 1.2 to 1.5 ns are observed. Thus, we can reasonably conclude that overall the photophysical properties of ^{H}**TIPP_BF$_2$** in different solvents are very similar, and consequently there is only a minor solvent effect in action here. We then opted for performing the following measurements on ^{R}**TIPP_BF$_2$** compounds in dichloromethane, which is the best choice in terms of solvent power and measured photoluminescent quantum yield (Table 1).

The normalized UV–vis spectra (CH_2Cl_2, $5{\cdot}10^{-5}$ M) for all ^{R}**TIPP_BF$_2$** compounds (Fig. 3, Fig. S36) are characterized by two absorption bands at about 240 and 280–290 nm and a lower energy absorption in the wavelength range between 320 nm and 340 nm (Table 2).

The normalized excitation and emission spectra recorded in solution (CH_2Cl_2, $5{\cdot}10^{-5}$ M) for ^{R}**TIPP_BF$_2$** are shown in Fig. 4. The excitation spectra (Fig. 4, dashed lines) perfectly duplicate the absorption traces of Fig. 3; all the emission maxima (Fig. 4, solid lines) are positioned in the near-UV range (357–390 nm), and λ_{max} is influenced by the *para*-substituent R to the hydroxyl group of the phenolic fragment. Indeed, emission maxima move to higher wavelengths with increasing the electron donating character of the substituent (i.e., from 357 for ^{H}**TIPP_BF$_2$** to 388 for ^{OH}**TIPP_BF$_2$** and 390 for ^{OMe}**TIPP_BF$_2$**). All complexes ^{R}**TIPP_BF$_2$** show a fluorescence behavior, with mono-exponential lifetime decays in the range of 1.1–1.4 ns (Table 2, Fig. S37). Absolute quantum yields are high for ^{H}**TIPP_BF$_2$**, ^{Me}**TIPP_BF$_2$** and ^{OMe}**TIPP_BF$_2$** derivatives, the latter showing a large enhancement in Φ_{PL} (0.49) when compared to the value recorded for free 4-methoxy-2-(1-methyl-5,6,7,8-tetrahydroimidazo[1,5-*a*]pyridin-3-yl)phenol ^{OMe}**TIPP** [0.11, see Ref. 21]. On the contrary, ^{F}**TIPP_BF$_2$** photoluminescence quantum yield is lower and experiences a considerable diminution with respect to the organic counterpart 4-fluoro-2-(1-methyl-5,6,7,8-tetrahydroimidazo[1,5-*a*]pyridin-3-yl)phenol ^{F}**TIPP** (0.30 *vs.* 0.72) [21].

Notably, despite the absorption wavelength of these compounds is short, they all showed good optical stability in solution when irradiated with high-energy UV light. As an example, compound ^{H}**TIPP_BF$_2$** was subjected to a multiple scan experiment: several emission spectra were repeatedly collected in dichloromethane solution (λ_{exc} 319 nm, 100 scans, no interval between scans; see Fig. S38). The shapes of the spectra obtained were nearly identical, with λ_{em} always being centered at 357

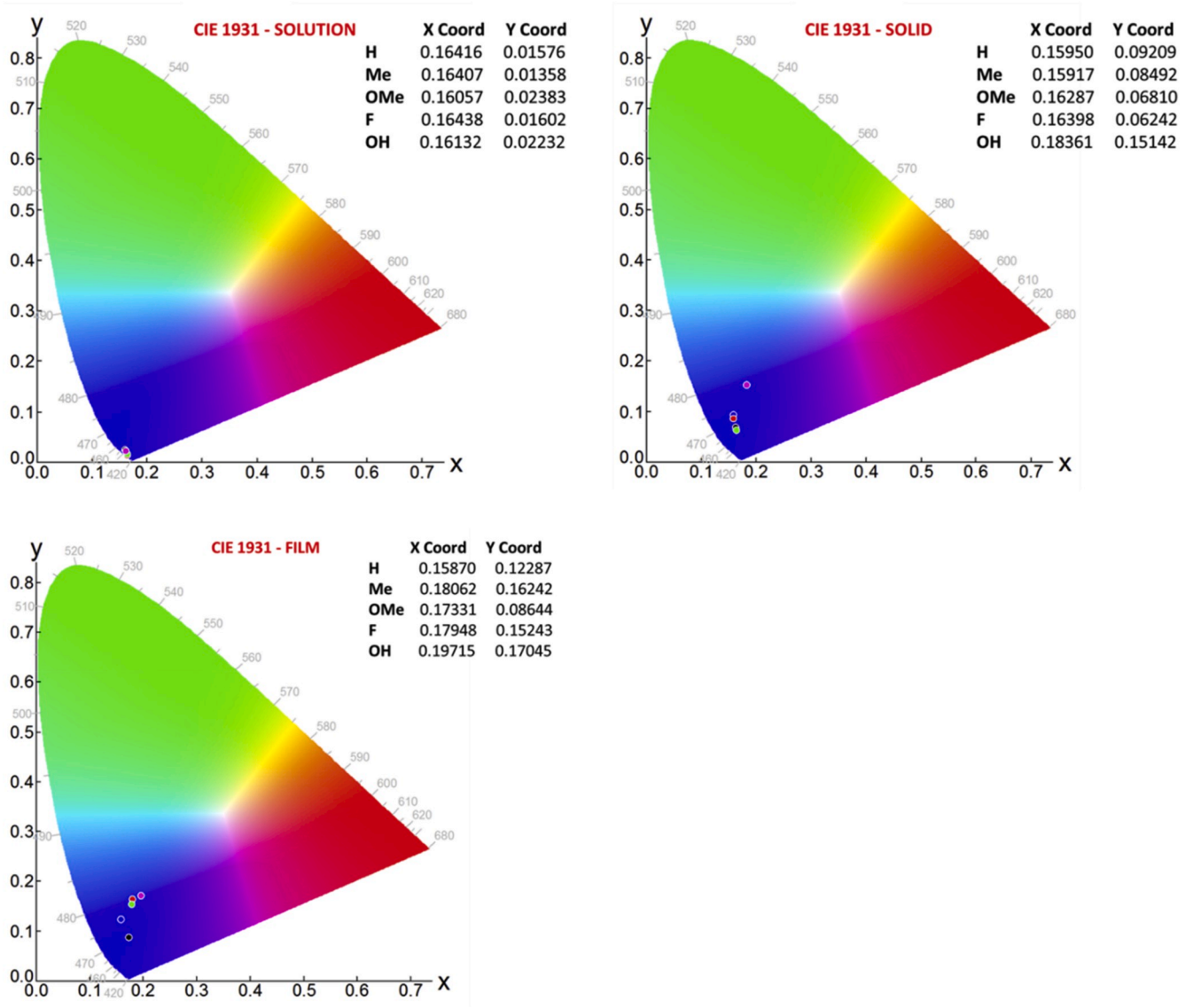

Fig. 5. CIE 1931 chromaticity plots for emission of compounds ^{R}**TIPP_BF$_2$** in solution (top left), in solid state (top right) and as thin layer (bottom left).

nm, whereas the intensity of the signal lessened of only 3.49% after 100 scans (= 100 min of irradiation) (Fig. S39).

The boron difluoride complexes ^{R}**TIPP_BF$_2$** show as well a bright emission in the solid state (Table 3, Figs. S40–S41). Both excitation and emission maxima are red-shifted with respect to those in solution, respectively of about 25 nm (excitation) and 30–50 nm (emission). Photoluminescence quantum yields are similar to those observed in dichloromethane solution, with the exception of the fluoride derivative ^{F}**TIPP_BF$_2$** which shows a significant increase moving from $\Phi_{PL} = 0.30$ (solution) to $\Phi_{PL} = 0.48$ (solid state). Fluorescence lifetime decays are slightly longer than in solution (6–7 ns) (Fig. S42); those derivatives with strong electron-donating substituents on the phenolic ring, namely ^{OMe}**TIPP_BF$_2$** and ^{OH}**TIPP_BF$_2$** show multi-exponential decay curves, probably due to crystallographic independence of some fragments and/or heterogeneity in (tetrahydroimidazo[1,5-*a*]pyridin-3-yl)phenol surrounding as already encountered previously [20].

As mentioned, all these new species have in the solid state an emission λ_{max} centered in the deep blue region, as documented by the corresponding CIE1931 plot (Fig. 5). Notably, the corresponding *x*,*y* coordinates are close to those expected for standard blue [1], thus suggesting the potential use of these species ^{R}**TIPP_BF$_2$** as blue emissive materials in optoelectronic devices.

The shape of excitation and emission spectra recorded as thin layer when these compounds have been dispersed in a host polymeric matrix such as poly(methyl methacrylate, PMMA) are quite similar to those recorded in solution (Figs. S43–S44). Lifetime decays are fitted with a bi-exponential curve, with τ_1 and τ_2 respectively in the range 1.0–1.3 and 2.5–4.6 ns (Fig. S45). Absolute quantum yields are slightly lower than in solution and in solid state. The different behavior of these derivatives observed between solution and solid state could be ascribed to different mechanisms of excited state relaxation, as indirectly corroborated by the different lifetime decays observed. The reduced quantum yields of boron difluoride compounds in PMMA films with respect to solution and solid state could be explained by possible self-absorption effects, which cannot be ruled out at 5% weight concentration of the dye in the host polymeric matrix, or some other interactions with the matrix itself favoring non-radiative decay paths. A systematic study on the effects on quantum yields of dye concentration when incorporated in PMMA films is in due course.

As previously done, compound ^{H}**TIPP_BF$_2$** was subjected to a multiple scan experiment also at the solid state to assess its photostability: sequential emission spectra were collected (λ_{exc} 343 nm, 45 scans, ca 3 min/scan, no interval between scans; see Fig. S46). Again, the spectra recorded showed a nearly identical profile, with λ_{em} always being

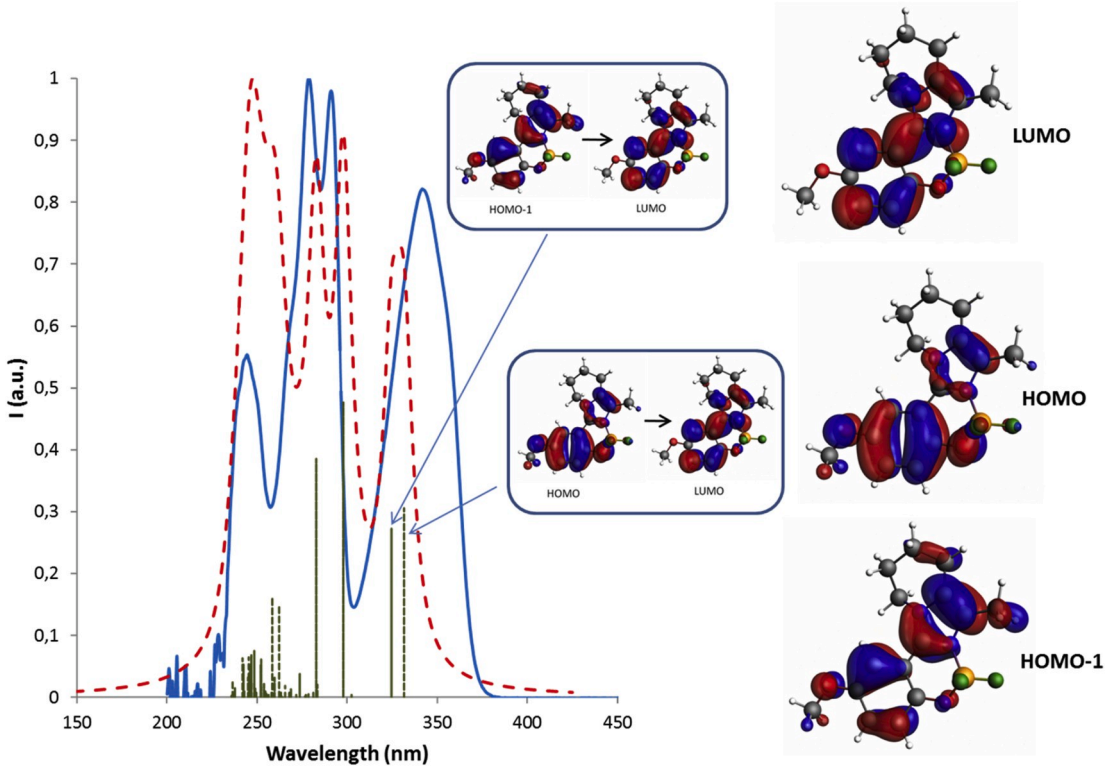

Fig. 6. Calculated (dashed red) *vs*. experimental (solid blue) UV–vis spectra (CH_2Cl_2, $5{\cdot}10^{-5}$ M) for compound ^{OMe}**TIPP_BF$_2$**, taken as a representative example of the series. On the right: HOMO, HOMO-1 and LUMO orbitals calculated for ^{OMe}**TIPP_BF$_2$**. (For interpretation of the references to color in this figure legend, the reader is referred to the Web version of this article.)

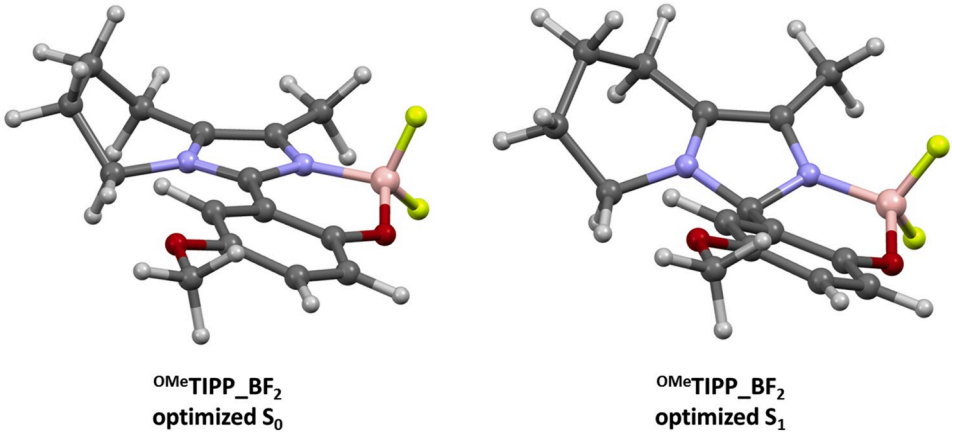

Fig. 7. Optimized geometries for the ground state (S_0) and excited state (S_1) for ^{OMe}**TIPP_BF$_2$**.

centered at 430 nm; a total loss of intensity of 12.76% was observed at the end of the experiment (= after 135 min of continuous irradiation) (Fig. S47), whereas the intensity loss after 100 min is about 10% (to be compared with 3.5% in solution).

4. DFT calculations

Starting from the X-ray data obtained for compound ^{OMe}**TIPP_BF$_2$**, we optimized the geometries of all ^{R}**TIPP_BF$_2$** derivatives at the DFT/PBE-D3 level of theory. Furthermore, TD-DFT calculations were performed to establish the nature of the transitions responsible for the absorption processes. The calculated UV–vis spectra in solution (CH_2Cl_2) are very close to the experimental ones (Fig. 6). The absorption at lower energy has been defined for all species as composed of two main transitions (>98%), namely HOMO/LUMO and HOMO-1/LUMO (Figure 6). The shape of the frontier orbitals is quite similar for all ^{R}**TIPP_BF$_2$** species: the HOMO and LUMO orbitals are spread over the organic fragment, with the exception of the methylenic groups, not involved in any transition. The HOMO-1 is mainly localized on the imidazolic ring of the tetrahydroimidazo-pyridine. Notably, nearly no contribution from BF_2 is observed, thus reasonably the role of the boron difluoride fragment is to enhance the photoluminescence performances (i.e., quantum yields) of the (tetrahydroimidazo[1,5-*a*]pyridin-3-yl)phenols by giving more rigidity to the system after coordination.

The geometries of both the ground state (S_0) and the excited state (S_1) of ^{OMe}**TIPP_BF$_2$** have been calculated in dichloromethane solution (Fig. 7). A great distortion of S_1 with respect to S_0 is observed. In the latter, the two planes defined by the phenolic residue and the imidazo-

pyridine portion are twisted only by 15.50°, whereas in S_1 the same angle measures 38.47° (Fig. S48, Supporting). As a consequence, the torsion angle between the two planes approaches nearly zero in S_0 (C13–N1–C7–C6 = 1.06°), while it measures 38.53° in S_1 (Fig. S49).

5. Conclusions

Herein we presented the synthesis of a series of BF_2-functionalized (tetrahydroimidazo[1,5-*a*]pyridin-3-yl)phenols with different substituents R in the *para* position to the hydroxyl group. These compounds show good absolute quantum yields, with general enhanced performances (i.e., quantum yields) due to the presence of the BF_2 fragment. One peculiar feature of these compounds is represented by their deep blue fluorescence emission, with *x*,*y* CIE coordinates close to those expected for a standard blue color. Additionally, multi scan experiments allowed to demonstrate that our boron difluoride complexes possess a quite good photostabilty in dichloromethane solution and at the solid state, with an intensity loss greater in solid state (10%) than in solution (3.5%) after 100 min of continuous irradiation with high-energy UV-light.

To sum up, the boron difluoride-functionalized (tetrahydroimidazo [1,5-*a*]pyridin-3-yl)phenols herein presented are characterized by *i*) deep blue emission in solution and solid state, with CIE 1931 color coordinates alike to standard blue; *ii*) absolute quantum yields up to 0.68; *iii*) good photostability under UV-light irradiation in solution and solid state. Additionally, they can be obtained by an easy two-steps synthesis starting from low-cost reagents and they show high solubility in common organic solvents. All things considered, to our eyes these compounds constitute an interesting class of blue emissive dyes which could be suitable for solution processable OLEDs application or Luminescent Solar Concentrators (LSCs). Finally, the presence of reactive functional groups (i.e., OH) in their skeleton leads to possible further functionalization, thus opening the way to new innovative emissive materials.

Declaration of competing interest

The authors declare that they have no known competing financial interests or personal relationships that could have appeared to influence the work reported in this paper.

CRediT authorship contribution statement

Gioele Colombo: Investigation, Writing - original draft. **Antonio Romeo:** Investigation. **G. Attilio Ardizzoia:** Conceptualization, Investigation, Writing - original draft, Funding acquisition. **Julien Furrer:** Investigation, Writing - original draft. **Bruno Therrien:** Investigation, Writing - original draft. **Stefano Brenna:** Writing - review & editing, Conceptualization, Investigation, Funding acquisition, Writing - original draft.

Acknowledgements

The authors thank the Ministero dell'Università e della Ricerca (MIUR) and the University of Insubria for funding. Fondazione Banca del Monte di Lombardia (FBML) is greatly acknowledged for generous funding through the Research Project "*Transiton-metals based coordination compounds for light emitting device applications*".

Appendix A. Supplementary data

Supplementary data to this article can be found online at https://doi.org/10.1016/j.dyepig.2020.108636.

References

[1] Lee J-H, Chen C-H, Lee P-H, Lin H-Y, Leung M-K, Chiu T-L, et al. Blue organic light-emitting diodes: current status, challenges, and future outlook. J Mater Chem C 2019;7:5874–88.
[2] Montanaro S, Congrave DG, Etherington MK, Wright IA. Homoconjugation enhances the photophysical and electrochemical properties of a new 3D intramolecular charge transfer iptycene displaying deep blue emission. J Mater Chem C 2019;7:12886–90.
[3] Konidena RR, Lee KH, Lee JY. Molecular design and synthetic approach to C2,C3, C4-modified carbazoles: high triplet energy bipolar host materials for efficient blue phosphorescent organic light emitting diodes. Chem Commun 2019;55:8178–81.
[4] Im Y, Byun SY, Kim JH, Lee DR, Oh CS, Yook KS, et al. Recent progress in high-efficiency blue-light-emitting materials for organic light-emitting diodes. Adv Funct Mater 2017;27:1603007.
[5] Chen WC, Lee CS, Tong QX. Blue-emitting organic electrofluorescence materials: progress and prospective. J Mater Chem C 2015;3:10957–63.
[6] Chen XK, Kim D, Brédas JL. Thermally activated delayed fluorescence (TADF) path toward efficient electroluminescence in purely organic materials: molecular level insight. Acc Chem Res 2018;51:2215–24.
[7] Huang T, Jiang W, Duan L. Recent progress in solution processable TADF materials for organic light-emitting diodes. J Mater Chem C 2018;6:5577–96.
[8] Tagare J, Vaidyanathan S. Recent development of phenanthroimidazole based fluorophores for blue organic light-emitting diodes (OLEDs): an overview. J Mater Chem C 2018;6:10138–73.
[9] [For representative examples]:. a) Fresta E, Volpi G, Garino C, Barolo C, Costa RD. Contextualizing yellow light-emitting electrochemical cells based on a blue-emitting imidazo-pyridine emitter. Polyhedron 2018;140:129–37.b) Yagishita F, Kozai N, Nii C, Tezuka Y, Uemura N, Yoshida Y, et al. Synthesis of dimeric imidazo [1, 5-a]pyridines and their photophysical properties. Chemistry 2017;2:10694–8. c) Shibahara F, Yamaguchi E, Kitagawa A, Imai A, Murai T. Synthesis of 1,3-diarylated imidazo[1,5-a]pyridines with a combinatorial approach: metal-catalyzed cross-coupling reactions of 1-halo-3-arylimidazo-[1,5-a]pyridines with arylmetal reagents. Tetrahedron 2009;65:5062–73.
[10] Volpi G, Magnano G, Benesperi I, Saccone D, Priola E, Gianotti V, et al. One pot synthesis of low cost emitters with large Stokes' shift. Dyes Pigments 2017;137:152–64.
[11] Chen S, Li H, Hou P. A large Stokes shift fluorescent probe for sensing of thiophenols based on imidazo[1,5-*a*]pyridine in both aqueous medium and living cells. Anal Chim Acta 2017;993:63–70.
[12] Salassa L, Albertino A, Garino C, Volpi G, Nervi C, Gobetto R, et al. Computational and spectroscopic studies of new rhenium(I) complexes containing pyridylimidazo [1,5-*a*]pyridine ligands: charge transfer and dual emission by fine-tuning of excited states. Organometallics 2008;27:1427–35.
[13] Garino C, Ruiu T, Salassa L, Albertino A, Volpi G, Nervi C, et al. Spectroscopic and computational study on new blue emitting ReL(CO)3Cl complexes containing pyridylimidazo[1,5-*a*]pyridine ligands. Eur J Inorg Chem 2008:3587–91.
[14] Weber MD, Garino C, Volpi G, Casamassa E, Milanesio M, Barolo C, et al. Origin of a counterintuitive yellow light-emitting electrochemical cell based on a blue-emitting heteroleptic copper(I) complex. Dalton Trans 2016;45:8984–93.
[15] Kundu N, Towsif Abtab SM, Kundu S, Endo A, Teat SJ, Chaudhury M. Triple-stranded helicates of zinc(II) and cadmium(II) involving a new redox-active multiring nitrogenous heterocyclic ligand: synthesis, structure, and electrochemical and photophysical properties. Inorg Chem 2012;51:2652–61.
[16] Guckian AL, Doering M, Ciesielski M, Walter O, Hjelm J, O'Boyle NM, et al. Assessment of intercomponent interaction in phenylene bridged dinuclear ruthenium(II) and osmium(II) polypyridyl complexes. Dalton Trans 2004:3943–9.
[17] Ardizzoia GA, Brenna S, Durini S, Therrien B, Veronelli M. Synthesis, structure, and photophysical properties of blue-emitting zinc(II) complexes with 3-aryl-substituted 1-Pyridylimidazo[1,5-*a*]pyridine ligands. Eur J Inorg Chem 2014:4310–9.
[18] Ardizzoia GA, Brenna S, Durini S, Therrien B. Synthesis and characterization of luminescent zinc(II) complexes with a N,N-bidentate 1-pyridylimidazo[1,5-a]pyridine ligand. Polyhedron 2015;90:214–20.
[19] Ardizzoia GA, Colombo G, Therrien B, Brenna S. Tuning the fluorescence emission and HOMO-LUMO band gap in homoleptic zinc(II) complexes with *N*,*O*-bidentate (Imidazo[1,5-*a*]pyrid-3-yl)phenols. Eur J Inorg Chem 2019:1825–31.
[20] Durini S, Ardizzoia GA, Therrien B, Brenna S. Tuning the fluorescence emission in mononuclear heteroleptic trigonal silver(I) complexes. New J Chem 2017;41:3006–14.
[21] Marchesi A, Brenna S, Ardizzoia GA. Synthesis and emissive properties of a series of tetrahydro (imidazo[1,5-*a*]pyrid-3-yl)phenols: a new class of large Stokes shift organic dyes. Dyes Pigments 2019;161:457–63.
[22] John A, Bolte M, Lerner H-W, Meng G, Wang S, Peng T, et al. Doubly boron-doped pentacenes as emitters for OLEDs. J Mater Chem C 2018;6:10881–7.
[23] Frath D, Massue J, Ulrich G, Ziessel R. Luminescent materials: locking p-conjugated and heterocyclic ligands with boron(III). Angew. Chem. Int. 2014;53:2290–310.
[24] Clarke R, Lok Ho K, Abdullah Alsimaree A, Woodford OJ, Waddell PG, Bogaerts J, et al. Circularly polarised luminescence from helically chiral "confused" N, N,O,C-Boron-Chelated dipyrromethenes (BODIPYs). ChemPhotoChem 2017;1:513–7.
[25] Boens N, Verbelen B, Ortiz MJ, Jiao L, Dehaen W. Synthesis of BODIPY dyes through post functionalization of the boron dipyrromethene core. Coord Chem Rev 2019;399:213024.
[26] Shimizu S. aza-BODIPY synthesis towards vis/NIR functional chromophores based on a Schiff base forming reaction protocol using lactams and heteroaromatic amines. Chem Commun 2019;55:8722–43.

[27] Bonardi L, Kanaan H, Camerel F, Jolinat P, Retailleau P, Ziessel R. Fine-tuning of yellow or red photo- and electroluminescence of functional difluoro-boradiazaindacene films. Adv Funct Mater 2008;18:401–13.
[28] Bessette A, Hanan GS. Design, synthesis and photophysical studies of dipyrromethene-based materials: insights into their applications in organic photovoltaic devices. Chem Soc Rev 2014;43:3342–405.
[29] Urban M, Durka K, Górka P, Wiosna-Sałyga G, Nawara K, Jankowski P, et al. The effect of locking π-conjugation in organoboron moieties in the structures of luminescent tetracoordinate boron complexes. Dalton Trans 2019;48:8642–63.
[30] Bonacorso HG, Calheiro TP, Iglesias BA, Acunha TV, Franceschini SZ, Ketzer A, et al. 1,1-Difluoro-3-aryl(heteroaryl)-1H-pyrido[1,2-c][1,3,5,2]oxadiazaborinin-9-ium-1-uides: synthesis; structure; and photophysical, electrochemical, and BSA-binding studies. New J Chem 2018;42:1913–20.
[31] Wu Y, Yuan W, Ji H, Qin Y, Zhang J, Li H, et al. New fluorescent imidazo[1,2-a] pyridine-BODIPY chromophores: experimental and theoretical approaches, and cell imaging exploration. Dyes Pigments 2017;142:330–9.
[32] Yagishita F, Kinouchi T, Hoshi K, Tezuka Y, Jibu Y, Karatsu T, et al. Highly efficient blue emission from boron complexes of 1-(*o*-hydroxyphenyl)imidazo[1,5-*a*] pyridine. Tetrahedron 2018;74:3728–33.
[33] Pålsson LO, Monkman AP. Measurements of solid-state photoluminescence quantum yields of films using a fluorimeter. Adv Mater 2002;14:757–8.
[34] Sheldrick GM. Phase annealing in SHELX-90: direct methods for larger structures. Acta Crystallogr 1990;A46:467–73.
[35] Sheldrick GM. Crystal structure refinement with SHELXL. Acta Crystallogr 2015; C71:3–8.
[36] Farrugia LJ. ORTEP-3 for windows - a version of ORTEP-III with a graphical user interface (GUI). J Appl Crystallogr 1997;30:565.
[37] a) te Velde G. Bickelhaupt FM, baerends EJ, fonseca guerra C, van Gisbergen SJA, snijders JG, ziegler T. Chemistry with ADF. J Comput Chem 2001;22:931–67.b) Fonseca Guerra C, Snijders JG, te Velde G, Baerends EJ. Towards an order-*N* DFT method. Theor. Chem. Acc 1998;99:391–403.c) Baerends EJ, Ziegler T, Autschbach J, Bashford D, Bérces A, Bickelhaupt FM, et al. ADF2014, SCM, theoretical chemistry, vrije universiteit, amsterdam, The Netherlands. http://www.scm.com.
[38] Grimme S, Antony J, Ehrlich S, Krieg S. A consistent and accurate *ab initio* parametrization of density functional dispersion correction (DFT-D) for the 94 elements H-Pu. J Chem Phys 2010;132:154104.
[39] Chong DP. Augmenting basis set for time-dependent density functional theory calculation of excitation energies: Slater-type orbitals for hydrogen to krypton. Mol Phys 2005;103:749–61.
[40] a) Klamt A, Schürmann GJ. COSMO: a new approach to dielectric screening in solvents with explicit expressions for the screening energy and its gradient. J. Chem. Soc. Perkin Trans. 1993;2:799–805.b) Klamt A, Jonas V. Treatment of the outlying charge in continuum solvation models. J Chem Phys 1996;105: 9972–81.c) Pye CC, Ziegler T. An implementation of the conductor-like screening model of solvation within the Amsterdam density functional package. Theor. Chem. Acc 1999;101:396–408.
[41] Ardizzoia GA, Ghiotti D, Therrien B, Brenna S. Homoleptic complexes of divalent metals bearing N,O-bidentate imidazo [1,5-*a*]pyridine ligands: synthesis, X-ray characterization and catalytic activity in the Heck reaction. Inorg Chim Acta 2018; 471:384–90.